



PERFORMANCEANALYSIS OF A HIGH GAINBIDIRECTIONAL DC-DC CONVERTER FEDDRIVE FOR AN ELECTRIC VEHICLE WITH BATTERY CHARGING CAPABILITY DURING BRAKING

¹T.Venkatesh, ²N.Leela Sowmya, ³S.Manindra, ⁴M.Yesu , ⁵K.venkatesh ¹Assisant Professor, ^{2,3,4,5} UG scholars

Department of Electrical & Electronics Engineering

Chalapathi Institute of Engineering and Technology, Guntur, Andhra Pradesh, India.

Email: manindrasingana@gmail.com

ABSTRACT: -This project presents a novel non-isolated high gain bidirectional DC-DC converter (BDC) and its application in integrating energy storage system with electric vehicle (EV). The proposed converter can provide high voltage gain with the help of two duty cycle operation by employing fewer components in its circuit design. The proposed topology makes use of dual current path inductor structures which reduces their size and eliminates the need for an additional clamping circuit to power the load. Without using voltage multiplier cells (VMC) or hybrid switched-capacitor approaches, the proposed converter can achieve a significant voltage gain. The simulation of the proposed converter-based drive is carried out using MATLAB/Simulinkthe performance analysis is done for different driving conditions. The converter powers the motor through the battery during the forward motoring mode. The motor acts as a generator during regenerative braking and the energy is transferred back through the converter to the battery which stores the recovered energy.

INDEX TERMS: Bidirectional dc–dc converter, high voltage gain, electric vehicle, regenerative braking, battery charging.

1.INTRODUCTION

Governmental bodies and organizations are enforcing stricter limits for fuel consumption and emissions due to the rising rate of oil consumption in the transportation sector, as well as growing concerns over the impact of global warming and the depletion of energy resources. By 2040, it is predicted that the yearly sales of EVs and Hybrid Electric Vehicles (HEVs) would surpass those of petrol and diesel vehicles, with sales of over 48 million [1]. The automobile industry is concentrating on the development of new technologies for the power train, battery, and charging infrastructure in response to the rising demand for vehicles with better fuel efficiency

and less impact on the environment. The installation of a high-energybattery pack and regenerative braking aid in extending the driving range and battery life of electric vehicles.

Power electronic converters find its application in drivetrain to modulate the power flow from battery to the propulsion motors and to facilitate regenerative braking in the reverse direction. To increase efficiency and power density, the drivetrain motor and propulsion inverter are made to operate at higher voltage [2]. To raise the battery voltage to the desired level, a boost converter is used. It also enhances the overall performance of the drivetrain by delinking the battery voltage and the inverter dc link voltage [3]. The DCDC convertermustbe bidirectional





because the forward mode will face transient and overload conditions during which power gets transferred from the battery to load and during the reverse mode, the battery pack is to be charged. Some battery and the inverter [4], [5] are: a) It reduces the stress on the inverter with an additional DC stage b) It adjusts the inverter supply voltage to increase the motor output, c) The cost and size of the battery can be reduced because of lower cell count requirement and d) system voltage and battery can individually designed by the manufacturers. This architecture thus enables versatile system designs for vehicles with various output characteristics. For instance, the battery nominal voltage in the 2010 Toyota Prius is about 200 V, while the DC-DC converter raises the voltage of the dc bus to about 650 V [2].

The most common BDC is the one with an isolated framework [2], [6], [7], [8], [9], [10], [11]. These isolated converters employ the high frequency transformer throughout the operation, increasing its losses and volume. Transformer core saturation [25] is another issue with this kind Additionally, of converter. many isolated converter configurations, such as LLC converters, CLLC converters and dual-activebridge (DAB) converters, which are the most prevalent kind of isolated BDCs, call for a significant number of active switches [10], [11]. Therefore, non-isolated BDCs are typically preferred when isolation is not mandatory. This is due its simple structure and low component count, which draw the attention of several researchers. They are suitable for some applications, such as the drive train of an electric vehicle, where size and weight are crucial considerations.

To attain high conversion ratios, non-isolated BDCs employ many circuit principles, including SEPIC/Cuk/Zeta, voltage multiplier cells, switching capacitors, and linked inductors. Due to their cascaded construction, SEPIC/Cuk/ Zeta converters have a low efficiency and higher voltage stress. BDCs can be designed using voltage multiplier cells; however, this is restricted by the high voltage across switches. BDCs [12], [13], [14] utilize switched capacitors that perform better, have a simpler construction, and require less control complexity. However, for high-gain applications, the circuit becomes progressively complex and is susceptible to losses with the growing number of switches and capacitors.

The system efficiency can be increased with hybrid topologies, but there is insufficient voltage gain and a greater ripple current [15] associated with few of these topologies. However, high conversion factors can be attained using hybrid architectures like SEPIC/quasi-Z source with switched capacitors [16], [17]. Conversion efficiency is nonetheless limited by a high component count and its inability to provide soft switching. Large ripple current at the LV side is a prevalent issue with all high gain non-isolated BDC circuits as it shortens the life and degrade the performance of the battery. Large capacitors can control input ripple current [18], but it is not the preferred option due to the added bulk and cost to the system. Interleaved DC-DC converter is a better option to reduce the input current ripple, but it has a lower voltage gain and more components [19].

Another significant advancement in this regard is the coupled inductor-based bidirectional converter (CIBDC) architecture [20], [21], [22], [23], [24], [25] that aims to achieve a high voltage conversion ratio. Contrary to transformer-based topologies, these coupled inductor-based systems [20] allow energy exchange at several instants during the course of a single time period. By carefully planning the circuit, switch current and voltage stress can be reduced as well. Clamping the coupled inductor's leakage energy and minimizing voltage spikes and stress across switches are major challenges in coupled inductor





topologies. By raising the coupled inductance at the low voltage side, the CIBDC proposed in [21] could minimize the current ripple. But it restricts the number of turns of other windings and in turn the voltage transfer ratio of the BDC. The CIBDC suggested in [24] employs two secondary coupled inductor branches to obtain a greater voltage conversion ratio and current sharing features in addition to soft switching. A non-isolated high gain converter for microgrids is suggested in [26], where coupled inductor is substituted by a normal inductor to make the topology appropriate for high voltage conversion application. However, it is unidirectional. The proposed converter is a modified version of the converter in [26] with capability bidirectional for electric vehicle applications.

II. PROBLEM FORMATION

- Need for Energy Efficiency in EV
 Systems: Investigating the challenges in
 achieving high energy conversion
 efficiency for bidirectional power transfer
 in electric vehicle drives, particularly
 during regenerative braking.
- Challenges in Voltage Gain: Identifying the limitations of conventional DC-DC converters in providing the required high voltage gain for efficient battery charging during braking.
- Dynamic Behavior and Control:

 Addressing the lack of studies on the performance and dynamic behavior of bidirectional converters under varying braking and drive conditions in electric vehicles.
- Thermal Management and Loss Reduction: Highlighting the difficulties in maintaining thermal stability and reducing power losses in high-gain converter designs for electric vehicles.

• Seamless Mode Transitions: Analyzing the complexity of ensuring smooth transitions between motoring and regenerative braking modes while maintaining system efficiency.

III.PROPOSED HIGH GAIN BIDIRECTIONAL DC-DCCONVERTER (HGBDC)

The proposed HGBDC shown in figure 1has four active power switches $(S_1, S_2, S_3, \text{ and } S_4)$, two identical inductors $(L_1 \text{ and } L_2)$, a diode (D_1) , and a capacitor (C_H) at the high voltage side. Diode D_1 helps in blocking the reverse voltage V_L appearing across the MOSFET while the switches S_1 and S_2 are conducting in boost mode. A switching frequency of f_s is used by the switches S_1 , S_2 , S_3 , and S_4 . During boost mode, switches S_1 and S_2 have a duty ratio of d_1 , and switch d_1 and switch d_2 . The duty ratio of the switch d_1 is d_2 during boost mode and it is d_3 during buck mode of operation of the converter.

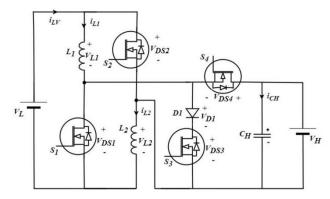


FIGURE 1. Proposed high gain bidirectional DC -DC converter (HGBDC).

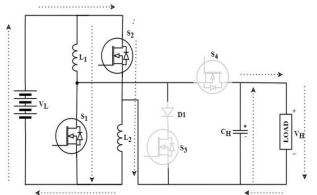
A. OPERATION OF THE HGBDC IN BOOST MODE

The boost operation of the converter is explained in three different phases namely, Mode I, Mode II and Mode III. The current flow path of the proposed HGBDC operating in boost mode is depicted in figure 2. During this mode, the energy





is transferred from the low voltage side to the high voltage side of the converter withthe help of



controlledswitches S_1 , S_2 , S_3 and S_4 . The switches S_1 , S_2 and S_3 are operated through the PWMcontrol. Typical waveforms of the proposed HG BDC in boost mode for continuous conduction are shown in figure 3.

1) MODE I

The switches S_1 and S_2 are turned on in this mode (t_0, t_1) , while the switches S_3 and S_4 are turned off for the duration of d_1T_s . Energy flow is from the battery to the inductors L_1 , L_2 which are connected in parallel, as shown in figure 2(a). The energy stored in the capacitor; C_H is released to the load. The voltage across the inductors is expressed in (1) to (3).

$$vL1 = vL2 = VL \tag{1}$$

$$LI\frac{diL1}{dt} = L2\frac{diL2}{dt} = L\frac{di}{dt} = VL$$
 (2)

$$\frac{diL}{dt} = \frac{VL}{L}$$
 (3)

where v_{L1} and v_{L2} are the voltages across inductors L_1 and L_2 respectively.

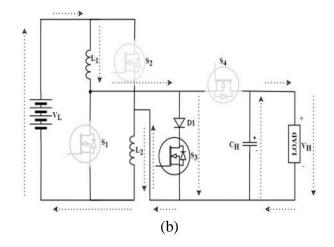
2) MODE II

Switch S_3 is active for the duration of d_2T_s , while switches S_1 and S_2 are turned off in Mode II (t_1 , t_2). As displayed in

figure 2(b), current flow is through L_1 , D_1 , S_3 and L_2 . The energy from the source is delivered to the inductors. The load receives the energy that is stored in the capacitor. Source is in series with the inductors in this mode. Equations (4) and (5) represent the currents flowing through and the voltages across the inductors.

$$i_{L1} = i_L 2$$
 (4)

(a)







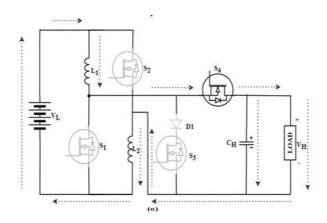


FIGURE 2. HGBDC in boost mode (a) Mode I (b) Mode II (c) Mode III.

where i_{L1} and i_{L2} are the current through inductors L_1 and L_2 respectively.

$$vL1 + vL2 = VL \tag{5}$$

$$v_{L1} = v_{L2} = L\frac{di}{dt} \tag{6}$$

$$\frac{diL}{dt} = \frac{VL}{2L} \tag{7}$$

3) MODE III

The MOSFET switches S_1 , S_2 and S_3 are turned off in this mode (t2, t3), whereas the body diode of the MOSFET S₄ conducts during (1-d₁-d₂)T_S. Diode D₁ is reverse biased. The load is supplied by both the source and the inductors as depicted in figure 2(c). The capacitor C_H is in charging mode

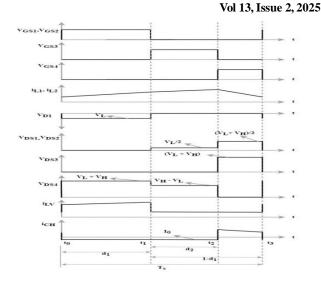


FIGURE 3. Operational waveforms of HGBDC in boost mode (CCM).

as the body diode of S₄ is forward biased. The inductors are connected in series to the source. The current through and the voltage across the inductors are given in (8) to (10).

$$i_{L1} = i_L 2$$
 (8)
 $vL1 + vL2 = VL - VH$ (9)
 $v_{L1} = v_{L2} = L\frac{diL}{dt}(10)$

From (9) and (10),

$$\frac{diL}{dx} = \frac{VL - VH}{2L} \quad (11)$$

(3), (7), and (11) are combined to get (12) using the state space averaging technique:

$$\int_{o}^{d1Ts} \left(\frac{diL}{dt}\right) + \int_{0}^{d2Ts} \left(\frac{diL}{dt}\right)^{II} dt + \int_{0}^{(1-d1-d2)Ts} \left(\frac{diL}{dt}\right)^{III} dt = 0$$
(12)





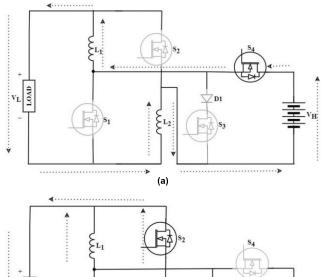


FIGURE 4. HGBDC in buck mode (a) Mode I (b) Mode II.

(b)

The modes of operation are indicated by the superscripts I, II, and III. The resulting voltage gain is given by (13).

$$\frac{V_H}{T} = \frac{(1+d_1)}{(1-d_1-d_2)}$$
(13)

B. OPERATION OF THE PROPOSED HGBDC IN BUCK MODE

The buck operation of the converter is explained in two different phases during the same switching cycle. The current flow path of the proposed HGBDC operating in buck mode is depicted in figure 4. Energy is transferred from the high voltage side to the low voltage side with the help of controlled switches S_4 , S_1 and S_2 in this mode. The switch S_4 is operated through the PWM control with a duty ratio of d_b . Operational waveforms of the proposed HGBDC in buck

mode for continuous conduction mode (CCM) are depicted in figure 5.

1) MODE I

In this mode (t_0 , t_1), S_4 is turned on and $S_1/S_2/S_3$ are turned off for a duration of d_bT_s . The inductors L_1 and L_2 , which are

connected in series with the load and the battery, facilitate the transfer of energy from the high voltage side to the low voltage side of the converter as shown in figure 4(a). Equations (14) to (16) give the current flowing through and the voltage across the inductors in this mode.

$$iL1 = iL2 \tag{14}$$

$$vL1 + vL2 = VH - VL \tag{15}$$

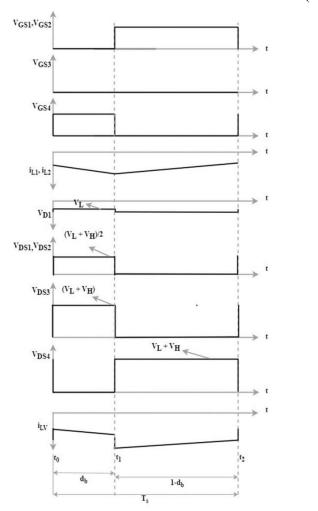


FIGURE 5. Operational waveforms of HGBDC in buck mode (CCM).





whereas,

$$vL1=vL2=L\frac{diL}{dt}$$

$$\frac{diL}{dt} = \frac{VH - VL}{2L} \quad (16)$$

2) MODE II

The body diodes of the MOSFETs S_1 and S_2 conduct for a duration of $(1-d_b)T_s$ in this mode $(t_1,$ t₂), while the MOSFET S₄ is turned off. Figure 4(b) depicts the current flow path. Inductors L₁ and L₂ discharge their stored energy to the load on low voltage side. Because L₁ and L₂ are in parallel, the voltages across them are as given in (17).

$$VL1=VL2=-VL$$
 (17)

$$L\frac{diL1}{dt} = L\frac{diL2}{dt} = -V2 \tag{18}$$

$$\frac{diL}{dt} = \frac{-Vl}{L} (19)$$

Equations (16) and (19) are combined to get (20) using the state space averaging technique.

$$\int_0^{dbTs} \left(\frac{diL}{dt}\right)^{I} dt + \int_0^{(1-db)} \left(\frac{diL}{dt}\right)^{II} dt = 0$$
 (20)

The modes of operation are indicated by the superscripts I and II. The resulting voltage gain in buck mode is given by (21).

$$\frac{\text{VL}}{VH} = \frac{db}{(2-db)} \quad (21)$$

where, d_bis the duty ratio of the HGBDC in buck mode of operation.

C. EFFICIENCY ANALYSIS

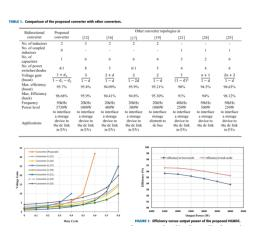
In order to determine the theoretical efficiency and compute converter losses, efficiency of the proposed converter is derived by taking the parasitic elements into consideration. To make the mathematical analysis simpler, the ripple in the capacitor voltage and inductor current is ignored. By taking these parasitic elements into consideration, the expression for voltage V_H at the high voltage side of the converter, is given by (22).

VH=
$$\frac{VL(1+d1)-VD1d2}{\frac{2(d1\propto 1+d2\propto 2+(1-d1-d2)\propto}{RH(1-d1-d2)}+(1-d1-d2)}$$
(22)

Where

$$\begin{cases} \propto = & rs1 + rL2 \\ \propto 2 = & \frac{rs3 + rL1 + rL2 + rD1}{2} \\ \propto 3 = & \frac{(rL1 + rL2 + rs4)}{2} \end{cases}$$

where, r_{L1} and r_{L2} are the ESR of the inductors L_1 and L₂ respectively. Similarly, r_{S1}, r_{S2}, r_{S3} and r_{S4} represent the ONstateresistancesoftheswitchesS₁,S₂,S₃ andS₄ respectively. r_{D1} and V_{D1} are the internal resistance and the voltage drop across the diode D₁ respectively. The resulting equation for efficiency of the proposed converter in boost mode of operation is given in (23).







$$\eta = PH PL = \frac{\frac{V^2}{RH} - Psw}{\frac{VLVH(1+d1)}{RH(1-d1-d2)}} (23)$$

where, P_H and P_L are the power at high voltage side and low voltage side of the converter respectively. R_H is the load resistance at high voltage side. P_{SW} is the switching loss across the power switches which is given by (24). The rise and fall time of the power switches are represented by t_r and t_f respectively.

$$PSW = 0.5V DSID tr + tffSW$$
 (24)

The expression for voltage V_L at the low voltage side of the converter, by taking the parasitic elements into consideration

FIGURE 6. Voltage gain versus duty cycle of the converters. is given in (25).

$$VL = \left(\frac{db}{2-db}\right) \frac{(2-db)^2 RL}{(2-db)^2 RL + db\beta 1 + 2(1-db)\beta 2}$$
(25)

where,

$$\beta 1 = rS4 + rL1 + rL2$$

$$\beta 2 = rL1 + rS1$$

The calculated efficiency of the proposed converter in stepdown mode is given by (26).

$$\eta = PL PH = \frac{\left(\frac{VL^2}{RL} - Psw\right)}{\frac{dbVLVH}{db(2-db)RL}} \quad (26)$$

where, R_L is the load resistance at low voltage side.

D. COMPARISONS WITH OTHER CONVERTERS

A comparison of the proposed converter with similar non isolated bidirectional converters is listed in Table 1. The comparison is made in terms of voltage gain, number of inductors, capacitors and switches, frequency of operation, power level, intended application and efficiency. The proposed HGBDC uses only four power switches and one diode, which is minimal when compared to the converters in [12], [16], [17], [19], and [25]. The number of inductors and capacitors are also least in comparison with the other converters. In Figure 6, the voltage gain against duty cycle is plotted for each of these converters. The voltage gain of the proposed HGBDC is higher than in other converters between a duty cycle range of 0.45 to 0.6 as can be seen in figure 6. The proposed HGBDC uses two different duty ratios 'd₁' and 'd₂' to achieve high voltage gain. With a constant duty ratio 'd2' as 0.35, 'd₁' is varied for plotting the graph. The converters in [24] and [25] use coupled inductors for which the turns ratio 'n' is taken as unity for plotting the graph. When duty ratio d_1 is at 0.6, the proposed HGBDC offers a high voltage gain of 32. However, the voltage gain of other converters are less than 15 for the same duty ratio.

TABLE 2. Parasitic parameters of components.

Parameter	Value	Parameter	Value
r _{S1,2,3,4}	$11 \mathrm{m}\Omega$	V_{D1}	0.83V
$V_{f1, 2,3, 4}$	1.4V	r_{D1}	$2.2 \mathrm{m}\Omega$
$t_{r1,2,3,4}$	30nS	r_{L1}	$24 \mathrm{m}\Omega$
$t_{f1,2,3,4}$	14nS	r_{L2}	$24 \mathrm{m}\Omega$

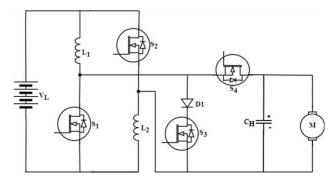


FIGURE 8. HGBDC connected to battery source and a dc motor load.

TABLE 3. Converter specifications.



Parameter	MATLAB/Simulink	RT-LAB
Input Voltage	48V	48V
Output Voltage	240V	240V
Switching Frequenc	50 kHz	5 kHz
Inductor L ₁ , L ₂	200 μΗ	1000 μΗ
Capacitor C _H	300 μF	1000 μF
Load (DC motor)	5 HP, 240 V,	5 HP, 240 V,
	1750rpm	1750 rpm

The efficiency of the proposed converter is calculated based on equations (23) and (26) for both boost and buck mode respectively. Table 2 lists the parasitic parameters of components for the MOSFET (IXFH120N30X3) and diode (STTH6004W)asgiveninthedatasheets.ESRofthei nductor is estimated to be 24 m • . The voltages at the high voltage side and low voltage side of the converter are 240V and 48V respectively. Theoretical efficiency curves in both boost and buck modes are plotted in figure 7. The calculated efficiency for a rated power of 3.73 kW is found to be 94.12% in boost mode and 95.51% in buck mode. The maximum efficiencies are 95.7% and 96.6% in boost and buck modes which are comparable to the efficiencies of the counterparts presented in Table 1 and better than that of the converter presented in [21]. Frequency, power level and intended application of the converters are also compared in Table 1. Even though the applications of the compared converters are meant for interfacing storage devices to the dc link, the performance analysis for the complete system is not discussed in the reference papers.

IV. CONVERTER DESIGN AND MOTOR CONTROL

The proposed HGBDC may be used to test its viability for applications like electric automobiles by integrating it into a simple DC motor drive. In this work, the converter is operated in continuous conduction mode to drive the dc motor in forward motoring and regenerative braking modes. The **HGBDC**

Parameter	Value/Specifications	
Туре	Li-ion	
Nominal Voltage	48 V	
Initial %SoC	80	
Battery Capacity	140 Ah	
Nominal Discharge Current	60.87 A	

is connected to a battery and a dc motor load as shown in figure 8. The light electric vehicle industry makes extensive use of DC motors, which are chosen for their simplicity and to check the viability of the converter operation in the proposed scheme. A 5 HP separately excited DC motor model rated at 240 V and 1750 rpm is utilized as the load to analyze the performance of the HGBDC in both MATLAB/Simulink and the real-time simulation mode. converter specifications are given in Table 3. The simulation makes use of the lithium ion (Li-ion) battery, whose specifications are listed in Table 4. The lithium-ion battery has a strong possibility of replacing other batteries as the foreseeable future of electric vehicle batteries. This is due to its fascinating properties including large power density, high energy density, extended life cycle, absence of memory effect, and superior energy efficiency. During regenerative braking, the proposed BDC transfers power from the motor back to the battery, and when the vehicle is moving, it delivers power from the battery to the DC motor.

A. INDUCTOR DESIGN

The selection of an inductor is influenced by the motoring mode of operation, which in turn depends on the input voltage (V_L), current ripple (I_{iL}) , frequency of switching (f_s) , and the duty cycle (d₁). The critical inductance value for the operation of the proposed HGBDC in CCM is determined using (27).





$$L1, critical = L2, critical = \frac{VLd1}{liLfs}$$
(27)

The inductor has been designed with 50 kHz switching frequency and a specified current ripple which is considered as 12% of the input current.

B. CAPACITOR DESIGN

The rated power (P_o) of the converter, load voltage (V_o), ripple voltage (IV_c), and the frequency of switching (f_s), are used to calculate the value of the capacitor, C_H on the high voltage side using (28).

$$Co, critical = \frac{P_o}{VolVcfs}$$
 (28)

A voltage ripple of 1% of the output voltage, V_H is used for the design of the capacitor.

C. VOLTAGE STRESS OF THE SWITCH **AND DIODE**

The voltage stress V_{DS1} , V_{DS2} , V_{DS3} and V_{DS4} across switches S₁ and S₂, S₃ and S₄ for boost mode of operation

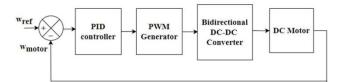


FIGURE 9. Block diagram of closed loop control scheme.

are given by (29), (30) and (31).

$$VH + VL$$

$$VDS1 = VDS2 = \underline{\qquad} \qquad (29)$$

$$VDS3 = VH \tag{30}$$

$$VDS4 = VH + VL \tag{31}$$

The voltage stress V_{D1} on the diode D_1 for both buck and boost mode of operations are given by equation (32).

$$V_{D1} = V_L + V_H (32)$$

The voltage stress V_{DS1}, V_{DS2}, V_{DS3} and V_{DS4} across switches S_1 and S_2 , S_3 and S_4 for buck operation are given in (33) and (34).

$$VDS1 = VDS2 = \frac{VH + VL}{2}$$
 (33)
$$VDS3 = VDS4 = VH + VL$$

(34)

D. CONTROL TECHNIQUE

A practical technique for adjusting the speed of the drive is to control the output voltage of the BDC. A PID controller is used to ensure that the vehicle reaches the target speed and reacts quickly to rapid changes in speed without oscillations. Figure 9 depicts the control circuitry for the HGBDC. It senses the motor speed ω_{motor} and compares it to the reference speed ω_{ref} . The error signal is processed by the PID controller and compared to a high-frequency sawtooth signal to generate the PWM control signals.

V. MODELLING AND SIMULATION **RESULTS**

The HGBDC fed DC motor drive is modelled and simulated using MATLAB/Simulink duration of 10 seconds. The steady-state inductor current and the gate drive pulses of the MOSFET switches for both boost and buck mode of operations of the converter are shown in figure 10 and figure 11 respectively. In boost (forward motoring) mode, the inductor current increases when the first three switches S_1 , S_2 and S_3 are turned on, whereas the current through the inductor decreases when the switch S4 is turned on. As shown in figure 10, the average value of the inductor current in steady state is 32 A. During buck (regenerative braking) mode, the



steady-state inductor current is -13.5A. Negative value of the inductor current shows the reversal of current flow from the load to source; hence the power flow. Battery is charged from the regenerative power during this braking mode. For a rated speed of 1750 rpm in forward motoring mode, the duty ratio of the PWM pulses generated by the PWM controller, d_1 and d_2 for the switches S_1/S_2 and S_3 respectively are 0.455 and

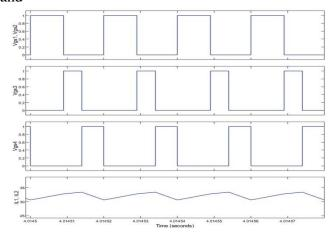


FIGURE 10. Switching signals for S_1 , S_2 , S_3 , S_4 and inductor currents in boost mode of operation

The converter is made to operate in boost (forward motoring) mode from 0-5 seconds and in buck (regenerative braking) mode from 5–10 seconds. Figure 12 shows the motor speed, armature torque, armature current, armature voltage (output voltage V_H) of the converter, battery SoC and battery voltage

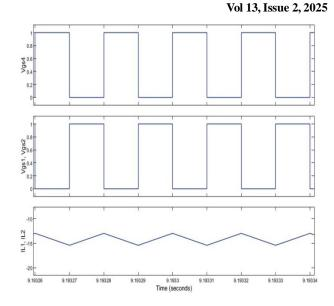


FIGURE 11. Switching signals for S_1 , S_2 , S_3 , S_4 and inductor currents in boost mode of operation.

0.245 for a voltage gain of 4.85. During regenerative braking mode, the switch S_4 operates with a duty ratio d_b which is 0.5 and the corresponding voltage gain is 1/3 for a speed of 1150 rpm.

Two different cases are considered for analyzing the dynamics of the system:

- (i) transition of the motor operation from forward motoring to regenerative braking.
- (ii) a step change in speed during forward motoring

A. TRANSITION OF THE MOTOR OPERATION FROM FORWARD MOTORING TO REGENERATIVE BRAKING

The converter is made to operate in boost (forward motoring) mode from 0-5 seconds and in buck (regenerative braking) mode from 5–10 seconds. Figure 12 shows the motor speed, armature torque, armature current, armature





voltage (output voltage V_H) of the converter, battery SoC and battery voltage

for this case. Simulations are carried out for the brakingaction with a speed change from 1750 rpm to 1150 rpm when the motor current and torque exhibit a reversal characteristic as shown in figure 12(a), 12(b) and 12(c) respectively. The change in directions of current and torque during the transition from motoring mode to regenerative braking mode indicates the reversal of power flow. As seen in figure 12(d)

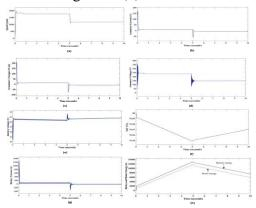


FIGURE 12. Simulation results for case 1-transition of the motor from forward motoring to regenerative braking (a) speed, (b) armature current, (c) armature torque, (d) armature voltage,

B. A STEP CHANGE IN SPEED DURING FORWARD MOTORING

Astep change in motor speed from 1250 RPM to 1750 RPM at constant torque constitutes the second instance of transient operation. Figure 13(a) depicts the speed waveform for a duration of 10 seconds. It is observed that the system settles down at the new speed within 0.5 seconds. The momentary change in armature torque caused by a sudden alteration in the speed is seen in Figure 13(c). The characteristics of current that is identical to that of torque is shown in figure 13(b). The change in armature voltage with respect to the change in motor speed is depicted

(e) battery SoC, (f) battery voltage, (g) battery current and (h) battery

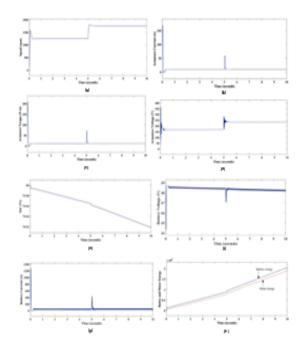


Figure 13. Simulation results for case 2 -transition of the motor from

forward motoring to regenerative braking (a) speed, (b) armature current, (c) armature torque, (d) armature voltage, (e) battery SoC, (f) battery voltage, (g) battery current and (h) battery

in figure 13(d). As seen in figure 13(e), when the speed increases, the motor draws more energy from the source, resulting in a fall in the SoC of the battery by 0.08%. The battery voltage and current during this phase are depicted in figures 13(f) and 13(g) respectively.

VI.CONCLUSION

This paper focused on the design and development of a High Gain Bidirectional Converter (HGBDC) for electric vehicle applications with battery charging capability during regenerative braking. The performance analysis of the converter is carried out during





motoring and regenerative braking modes in both MATLAB/SimulinkThe proposed method is simpler and the converter can attain high gain with the help of two duty cycle operation. It demonstrates a good balance among the voltage gain and the component counts which gives a viable solution to the application of interfacing storage devices to the DC link in electric vehicles which is the focus of the paper. The HGBDCalso successfully controls the power flow direction by modifying the converter's working mode from motoring to regenerative braking. The efficiency of the proposed converter can further be improved by selecting SiC based power switches. Further Soft switching can be implemented to reduce the switching losses when the converter operates at higher frequency, but it adds complexity and increases the number of components.

REFERENCES

[1] C. H. T. Lee, W. Hua, T. Long, C. Jiang, and L. V. Iyer, "A critical review of emerging technologies for electric and hybrid vehicles," IEEE Open J. Veh. Technol., vol. 10.1109/OJVT.2021.3138894. 2, pp. 471–485, 2021, doi: [2] V. Rathore, K. Rajashekara, P. Nayak, and A. Ray, "A high-gain multilevel DC–DC converter for interfacing electric vehicle battery and inverter," IEEE Trans. Ind. Appl., vol. 58, no. 5, pp. 6506–6518, Sep. 2022, doi: 10.1109/TIA.2022.3185183.

- [3] H. Chen, H. Kim, R. Erickson, and D. Maksimovic, "Electrified automotive powertrain architecture using composite DC–DC converters," IEEE Trans. Power Electron., vol. 32, no. 1, pp. 98–116, Jan. 2017, doi: 10.1109/TPEL.2016.2533347.
- [4] A. Gupta, R. Ayyanar, and S. Chakraborty, "Novel electric vehicle traction architecture with 48 V battery and multi-input, high conversion

ratio converter for high and variable DC-link voltage," IEEE Open J. Veh. Technol., vol. 2, pp. 448–470, 2021, doi: 10.1109/OJVT.2021.3132281.

[5] J. O. Estima and A. J. M. Cardoso, "Efficiency analysis of drive train topologies applied to electric/hybrid vehicles," IEEE Trans. Veh. Technol., vol. 61, no. 3, pp. 1021–1031, Mar. 2012, doi: 10.1109/TVT.2012.2186993. [6] D. Sha, D. Chen, and J. Zhang, "A bidirectional three-level DC–DC converter with reduced circulating loss and fully ZVS achievement for battery charging/discharging," IEEE J. Emerg. Sel. Topics Power Electron., vol. 6, no. 2, pp. 10.1109/JESTPE.2017.2778039. 993–1003, Jun. 2018, doi:

[7] T. Zhu, F. Zhuo, F. Zhao, F. Wang, H. Yi, and T. Zhao, "Optimization of extended phase-shift control for full-bridge CLLC resonant converter with improved light-load efficiency," IEEE Trans. Power Electron., vol. 35, no. 10, pp. 11129–11142, Oct. 2020, doi: 10.1109/TPEL.2020.2978419.

- [8] Y. Shen, H. Wang, A. Al-Durra, Z. Qin, and F. Blaabjerg, "A bidirectional resonant DC–DC converter suitable for wide voltage gain range," IEEE Trans. Power Electron., vol. 33, no. 4, pp. 2957–2975, Apr. 2018, doi: 10.1109/TPEL.2017.2710162.
- [9] C. Bai, B. Han, B.-H. Kwon, and M. Kim, "Highly efficient bidirectional series-resonant DC/DC converter over wide range of battery voltages," IEEE Trans. Power Electron., vol. 35, no. 4, pp. 3636–3650, Apr. 2020, doi: 10.1109/TPEL.2019.2933408.
- [10] N. Hou and Y. W. Li, "Overview and comparison of modulation and control strategies for a non resonant single-phase dual-active-bridge DC–DC converter," IEEE Trans. Power Electron., vol. 35, no. 3, pp. 3148–3172, Mar. 2020, doi: 10.1109/TPEL.2019.2927930.



[11] F. Zahin, A. Abasian, and S. A. Khajehoddin, "An alternative dual active bridge modulation to minimize RMS current and extend ZVS range," in Proc. IEEE Energy Convers. Congr. Exposit. (ECCE), Detroit, MI, USA, Oct. 2020, pp. 5952-5959, doi: 10.1109/ECCE44975.2020. 9235374.

[12] Y. Zhang, W. Zhang, F. Gao, S. Gao, and D. J. Rogers, "A switchedcapacitor interleaved bidirectional converter with wide voltage gain range for super capacitors in EVs," IEEE Trans. Power Electron., vol. 35, no. 2, pp. 1536-1547, Feb. 2020, doi: 10.1109/TPEL.2019. 2921585.

[13] Y. Zhang, Y. Gao, L. Zhou, and M. Sumner, "A switched-capacitor bidirectional DC-DC converter with wide voltage gain range for electric vehicles with hybrid energy sources," IEEE Trans. Power Electron., vol. 33, no. 11, pp. 9459-9469, Nov. 2018, doi: 10.1109/TPEL.2017.2788436.

[14] S. T. S. Lee, S. Y. R. Hui, W. C. Chow, and H. S. H. Chung, "Development of a switchedcapacitor DC-DC converter with bidirectional power flow," IEEE Trans. Circuits Syst. I, Fundam. Theory Appl., vol. 47, no. 9, pp. 1383– 1389, Sep. 2000, doi: 10.1109/81.883334.

[15] D. F. Cortez, G. Waltrich, J. Fraigneaud, H. Miranda, and I. Barbi, "DC- DC converter for dual-voltage automotive systems based bidirectional hybrid switched-capacitor architectures," IEEE Trans. Ind. Electron., vol. 62, no. 5, pp. 3296–3304, May 2015, doi: 10.1109/TIE.2014.2350454.

[16] Y. Zhang, Q. Liu, Y. Gao, J. Li, and M. Sumner, "Hybrid switchedcapacitor/switchedquasi-Z-source bidirectional DC-DC converter with a wide voltage gain range for hybrid energy sources EVs," IEEE Trans. Ind. Electron., vol. 66, no. 4, pp.2680–2690, Apr. 2019, doi: 10.1109/TIE.2018.2850020.

[17] A. Kumar, X. Xiong, X. Pan, M. Reza, A. R. Beig, and K. A. Jaafari, "A wide voltage gain bidirectional DC-DC converter based on quasi Z-

source and switched capacitor network," IEEE Trans. Circuits Syst. II, Exp. Briefs, vol. 68, no. 4, pp. 10.1109/TCSII.2020.3033048. 1353–1357, Apr. 2021, doi:

[18] Z. Wang, P. Wang, B. Li, X. Ma, and P. Wang, "A bidirectional DC- DC converter with high voltage conversion ratio and zero ripple current for battery energy storage system," IEEE Trans. Power Electron., vol. 36, no. 7, pp. 8012– 8027, Jul. 2021, doi: 10.1109/TPEL.2020.3048043.

[19] Y. Zhang, Y. Gao, J. Li, and M. Sumner, "Interleaved switchedcapacitor bidirectional DC-DC converter with wide voltage-gain range for energy storage systems," IEEE Trans. Power Electron., vol. 33, no. 5, pp. 3852 3869, May 2018, doi: 10.1109/TPEL.2017.2719402.

[20] L.-S. Yang and T.-J. Liang, "Analysis and implementation of a novel bidirectional DC-DC converter," IEEE Trans. Ind. Electron., vol. 59, Jan. 1, pp. 422–434, 2012, doi: 10.1109/TIE.2011.2134060.

[21] A. R. N. Akhormeh, K. Abbaszadeh, M. Moradzadeh, and A. Shahirinia, "High-gain bidirectional quadratic DC-DC converter based on coupled inductor with current ripple reduction capability," IEEE Trans. Ind. Electron., vol. 68, no. 9, pp. 7826–7837, Sep. 2021, 10.1109/TIE.2020.3013551.

[22] B. Li, P. Wang, Z. Wang, X. Ma, and H. Bi, coupled-inductor-based "A high-gain interleaved DC-DC converter with sustained soft switching," IEEE Trans. Veh. Technol., vol. 70, 7, pp. 6527–6541, Jul. 2021, 10.1109/TVT.2021.3083317.

[23] Y. Zhang, H. Liu, J. Li, and M. Sumner, "A low-current ripple and wide voltage-gain range bidirectional DC-DC converter with coupled inductor,"

IEEETrans.PowerElectron.,vol.35,no.2,pp. 1525– 1535,Feb.2020,doi:

10.1109/TPEL.2019.2921570.





[24] M. Das and V. Agarwal, "Design and development of a novel high voltage gain, high-efficiency bidirectional DC–DC converter for storage interface," IEEE Trans. Ind. Electron., vol. 66, no. 6, pp. 4490–4501, Jun. 2019, doi: 10.1109/TIE.2018.2860539.

[25] S. B. Santra, D. Chatterjee, and T.-J. Liang, "High gain and high-efficiency bidirectional DC–DC converter with current sharing characteristics using coupled inductor," IEEE Trans. Power Electron., vol. 36, no. 11, pp. 12819–12833, Nov. 2021, doi: 10.1109/TPEL.2021.3077584.

[26] M. Lakshmi and S. Hemamalini, "Nonisolated high gain DC–DC converter for DC microgrids," IEEE Trans. Ind. Electron., vol. 65, no. 2, pp. 1205 1212, Feb. 2018, doi: 10.1109/TIE.2017.2733463.